Low-Field High-Resolution PFG-NMR to Predict the Size Distribution of Inner Droplets in Double Emulsions

Behnam Khadem, Andrew Parrott, Alison Nordon, Nida Sheibat-Othman

Low-field high-resolution PFG-NMR to predict the size distribution of inner droplets in double emulsions

Behnam Khadem[a], Andrew Parrott[b], Alison Nordon[b], Nida Sheibat-Othman[a,*]

[a]Univ Lyon, Université Claude Bernard Lyon 1, CNRS, LAGEPP UMR 5007, F-69100, Villeurbanne, France.
[b]WestCHEM, Department of Pure and Applied Chemistry and Centre for Process Analytics and Control Technology, University of Strathclyde, Glasgow, G1 1XL, United Kingdom.
[*]corresponding author: nida.othman@univ-lyon1.fr

Abstract

In double emulsions, the inner and outer droplet size distribution determine the quality of the double emulsion and are therefore essential to be measured. Low-field high-resolution pulsed-field gradient nuclear magnetic resonance (PFG-NMR) is used to measure the inner droplet size distribution in water-in-oil-in-water double emulsions. The Gaussian Phase Distribution (GPD) approach is employed with a mixture of two normal distributions to predict bimodal inner droplets. This approach allowed to predict the swelling of inner droplet during storage of double emulsions, and thus to validate a phenomenological population balance model estimating inner droplet swelling. Only a fraction of the inner droplets was found to swell during storage, due to differences in the Laplace pressure, thus leading to the formation of a bimodal size distribution of the inner droplets. This methodology is useful to predict the evolution of double emulsions during storage, in a wide range of applications, such as food and pharmaceutical products.

Keywords: Droplet size distribution, PGF-NMR, Double emulsions, Modelling, Inner droplets

1. Introduction

Double emulsions, or emulsions of emulsions, have potential in a wide range of applications such as low-fat food products [1], encapsulation of active agents in pharmaceutical products

[2] or in extraction processes for instance for wastewater treatment [3]. Double emulsions are usually produced in two steps: the first step consists of the preparation of a primary emulsion by employing a high mixing energy; in a second step the primary emulsion obtained is dispersed into an external phase under a lower mixing energy [4]. While in simple emulsions the quality and the physical stability of the emulsion are governed by the droplet size distribution (DSD), in double emulsions the quality and physical stability depend on both the inner and outer DSDs. These properties are determined by the operating conditions, such as the agitation speed and duration, the concentrations of internal and external stabilizers, the viscosity of the different phases and the concentration of ions. Moreover, after preparation, different phenomena may occur leading to changes in the inner and outer DSDs and in the encapsulation efficiency, such as swelling/shrinkage, escape of inner droplets, coalescence and molecular diffusion. It is therefore essential to develop experimental methods to measure the key product qualities, i.e., the inner and outer DSD and the encapsulation efficiency. In parallel, it is important to develop phenomenological models allowing to predict the evolution of double emulsions during preparation and storage and to relate their properties to the operating conditions.

Measurement of the inner droplet size distribution. After the preparation of a double emulsion, the measurement of the outer DSD can be realized using conventional quantitative devices of simple emulsions, such as laser diffraction, with simple adaptations of few parameters, such as the refractive index. However, the measurement of the inner DSD represents a real challenge, as they are encapsulated within the outer droplets and the laser diffraction method would mainly be sensitive to the outer droplets. Regarding microscopy, a high resolution is required to observe the inner droplets as they usually have a submicron size. Optical microscopic visualization is limited to droplets bigger than 1 μm in diameter for light microscopes and to droplets bigger than 750 nm for confocal laser

scanning microscopy (CLSM), also referred to as fluorescence microscopy [5]. CLSM though represents a promising method to observe qualitatively the inner droplets, as quantitative description would require to analyze a big number of droplets [6–8].

Pulsed-field gradient nuclear magnetic resonance (PFG-NMR). Another method that was proposed to be sensitive to the inner droplet size is pulsed-field gradient nuclear magnetic resonance (PFG-NMR)[9–11]. This method measures signal attenuation arising from free and restricted self-diffusion of molecules, and this last one is dependent on the size of cavities [5–7,12–15]. However, a mathematical model is needed to predict the droplet size distribution from the measured signal attenuation. Several modelling approaches were suggested to relate the measured signal attenuation to the self-diffusion coefficient within spherical cavities, including: Short Gradient Pulse (SGP) [16], which assumes that no motion of the spins occurs during time that the field gradient pulses are applied, Gaussian Phase Distribution (GPD) [17], which assumes Gaussian distributed phases under the field gradient, and Block Gradient Pulse (BGP) approximation which is based on the solution of the Bloch–Torrey equation under steady gradient [18]. The BGP method allows coverage of the full range of gradient pulse durations and delays, while SGP and GPD perform adequately only in a specific range, but BGP needs heavier computations [19]. In practice, it is often not possible to obtain sufficiently short gradient pulses to fulfill the SGP condition. Therefore, we focus on the use of GPD in this work.

The earliest attempt to use PFG-NMR to measure the droplet size in double emulsions was done by Lönnqvist et al. (1997) [15] who employed the GPD approach to compare the DSD of water droplets in the primary emulsion (i.e., W/O) and in the final double emulsion (i.e., W/O/W) immediately after preparation. Both measurements were comparable indicating that only little alteration of the inner droplet size occurred during the second step of preparation of the double emulsion. In their conditions, the effect of free diffusion of the

continuous phase on signal attenuation was found negligible, therefore the methodology assumes only restricted diffusion. Pfeuffer et al. (1998) [20] introduced the concept of restricted interacellular diffusion at permeable boundaries, which assumes two exchanging components: one free diffusing and the other restricted. A comparable approach was proposed by Price et al. (1997) [21], but assuming the signal intensity of the internal compartment not to depend on the diffusion coefficient of internal molecules. These models assume that molecules may exchange between the inner droplets/cells and the external phase, thus the signal attenuation is described by a sum of signals from both compartments, with modified diffusion coefficients. Hindmarsh et al. (2005) [12] compared the exchange models of Pfeuffer et al. (1998) [20] and Price et al. (1998) [22] and obtained a better representation of the experiments using the Pfeuffer et al. model. Wolf et al. (2009) [5] also applied the exchange model of Pfeuffer et al. with the GPD approach and suggested that the external water in highly concentrated double emulsions requires specific considerations and cannot be considered as a continuous phase with simple free diffusion. In the same group, Guan et al. (2010) [13] evaluated molecular exchange between the inner and external water phases during the NMR measurement for recipes containing different amounts of Xanthan and/or sugar in the internal and/or external phases. They found that the addition of Xanthan to the external phase could eliminate water exchange while for all the other recipes exchange was observed within the time scale of the NMR measurement. They also reported slower molecular exchange for smaller inner droplets. This observation can be related to the higher Laplace pressure of smaller droplets. Vermeir et al. (2016) [14,23] found that exchange occurs from the inner water phase to the oil phase while diffusion to the external water phase was negligible during the NMR measurement.

Objectives. In this study, low-field (1 T) high-resolution PFG-NMR spectroscopy is employed to predict the inner size distribution in W/O/W double emulsions during storage. The

emulsions were prepared by high speed rotor-stator mixer and stored at room temperature. It was observed by laser diffraction that the double emulsions swell during storage at ambient temperature and reach a maximum of swelling after one week, after which they undergo overswelling breakdown [24]. Moreover, it was observed by optical microscopy that only a fraction of the inner droplets swells, thus leading to a bimodal inner DSD. This was explained by the fact that smaller droplets have a higher Laplace pressure, which works against their swelling. Therefore, the NMR mathematical treatment needs to be extended to a bimodal distribution. Thus, the Gaussian Phase Distribution (GPD) approach employed by Lönnqvist et al. (1997) [15] is considered in this work and adapted to bimodal distributions of inner droplets as suggested by van Duynhoven et al. (2002) [25] and Peña and Hirasaki (2003) [26]. Both free and restricted diffusions are considered in the model as suggested in the exchange model of Pfeuffer et al. (1998) [20]. The measurement obtained by this approach was compared to a recently developed phenomenological model predicting the inner and outer DSDs and the release rate during storage of double emulsions, thus allowing its validation [27]. This model consists of a coupled population balance model (PBM) of inner and outer droplets and involves the phenomena of swelling and escape of inner droplets.

2. Materials and methods

Materials. The materials used to prepare the W/O/W double emulsions are mineral oil (Fisher Scientific), Span 80 (Alfa Aesar) as the hydrophobic internal emulsifier, Tween 80 (Fisher Scientific) as the hydrophilic external emulsifier, sodium chloride as the tracer and regulator of osmotic pressure and Millipore water (resistivity $\approx 18.2 \, m\,\Omega.cm$).

Preparation of the double emulsion. The primary emulsion is prepared by dispersing an aqueous solution of NaCl (30 % wt) in an oil phase composed of mineral oil (60 % wt) and Span 80 (10 % wt) using ULTRA-TURRAX operating at 12 000 rpm for 4 min. Then, the double

emulsion was prepared by dispersing the primary emulsion (10 % wt) into an external aqueous phase (89 % wt) containing Tween 80 (1 % wt) using ULTRA-TURRAX® operating at 3 400 rpm for 4 min. The encapsulation efficiency was found to be 29.4 % using conductivity measurements (A CDM210 Conductivity Meter, MeterLab®) immediately after preparation. The double emulsion produced was then stored at room temperature.

Droplet size measurement. Immediately after the preparation of the primary emulsion (i.e. single water in oil emulsion), the DSD of the inner droplets was measured using dynamic light scattering (Malvern Zetasizer Nano ZS®), by dilution into oil. The outer droplets DSD (in the double emulsion) was measured after the second step of preparation as well as during storage by means of laser diffraction (Mastersizer 3000®) by dilution into water.

NMR measurement. The NMR measurement was done using Magritek Spinsolve Carbon 43 MHz benchtop NMR (1 T) equipped with a gradient coil with a maximum strength of 0.16 T/m. The pulse sequence used was the stimulated echo (STE) version of the pulsed field gradient pulse (PFG) methodology[9,28]. Table 1 shows the NMR operating conditions.

Table 1. NMR operating conditions

NMR parameter	Value(s)	Unit
Gradient pulse duration (δ)	0.004 or 0.01	s
Gradient pulse delay and diffusion time (Δ)	Between 0.05 and 0.4	s
Gradient amplitude (g), linear in 32 steps	0.012 to 0.155	T/m
Number of steps	16 or 32	-
Number of scans	4 or 8	-

3. Theoretical investigations

In this section, first the mathematical treatment of signal attenuation in PFG-NMR measurements is adapted to predict a bimodal distribution of inner droplets. Second, a phenomenological model allowing the prediction of inner droplet swelling in double

emulsions during storage is presented. The DSDs of inner droplets predicted by both approaches are compared in the results section.

3.1 Inner DSD prediction by PFG-NMR

Using PFG-NMR, the diffusion of fluid molecules in a confined environment can give useful information about the micro-structural features of the environment [19]. In the case of simple and double emulsions, this can give information about the DSD and permeability. Indeed, since the internal water molecules undergo restricted diffusion (i.e. the diffusion is restricted by the walls of the droplets), the DSD of inner droplets can be obtained by mapping the water molecular displacement [19].

While NRM time-domain data is a well-established method, based on extracting the water signal by using T1/T2 weighting, in low-field high-resolution PFG-NMR the frequency domain is used. This allows using chemical shift resolution to unambiguously measure the water phase signal. The use of a benchtop instrument has the advantage that it could be placed in a laboratory or in industrial environment, unlike a typically high field instrument [29,30]. This relatively novel technique is finding an interest in literature [31–34].

Douglass and McCall [17] and Stejskal and Tanner (1965) [35] proposed methods to measure free diffusion of molecules by PFG-NMR; Murday and Cotts [10] adapted this method to measure self-diffusion of confined molecules. The signal attenuation, E, due to diffusion in spherical cavities of radius r is given by [10]:

$$\ln E(\delta, g, \Delta, r) = -\frac{2\gamma^2 g^2}{D} \sum_{m=1}^{\infty} \frac{1}{\alpha_m^4(\alpha_m^2 r^2 - 2)} \left\{ 2\delta - \frac{1}{\alpha_m^2 D} \left[2 + e^{-\alpha_m^2 D (\Delta-\delta)} - 2e^{-\alpha_m^2 D \delta} - 2e^{-\alpha_m^2 D \Delta} + e^{-\alpha_m^2 D (\Delta+\delta)} \right] \right\} \qquad 1$$

where δ is the gradient pulse duration (s), g the magnitude of the filed gradient (T m^{-1}), Δ the gradient pulse delay or the diffusion time (s), D the self-diffusion coefficient of the

dispersed inner droplets (m^2 s^{-1}), r the droplet radius (m), γ the gyromagnetic ratio (T^{-1}s^{-1}), and α_m is the mth roots of the following function:

$$\frac{1}{\alpha r} \, \mathcal{J}_{\frac{3}{2}}(\alpha r) = \mathcal{J}_{\frac{5}{2}}(\alpha r)$$

where $\mathcal{J}_n$ is the nth order Bessel function.

The self-diffusion coefficient, D, was approximated for pure water to be 2.5×10^{-9} m^2 s^{-1} at 28.5°C at which the NMR measurements were realized [36].

Assuming the system to have two water exchanging components, one is free diffusion and another restricted, the water signal gives rise to a quasi bi-exponential decay as a function of q^2 (with $q = \gamma g \delta$) and diffusion delay Δ [14,20]:

$$E_{\mathrm{p}}(\delta, g, \Delta, r) = \frac{I}{I_0} = p_{\mathrm{intra}} E_{\mathrm{intra}} + (1 - p_{\mathrm{intra}}) e^{-\gamma^2 g^2 D_e \left\{ \delta^2 \left(\Delta - \frac{\delta}{3} \right) + \frac{\varepsilon^3}{30} - \frac{\delta \varepsilon^2}{6} \right\}} \qquad 2$$

Where p_{intra} is the volume fraction of enclosed water (inner water phase) compared to the total water phase, D_e is the effective diffusion coefficient in the external water phase, I and I_0 are the signal intensities with and without the gradient pluses respectively and ε is the gradient ramp time (0.1 ms in our case, therefore the terms of ε in equation 2 are negligible).

The NMR signal attenuation of inner droplets, $E_{\mathrm{intra}}(\delta, g, \Delta, R)$, is proportional to each droplet volume, which gives [5,12,19]:

$$E_{\mathrm{intra}}(\delta, g, \Delta, r) = \frac{\int_0^{\infty} r^3 \, P(r) \, E(\delta, g, \Delta, r) \, dr}{\int_0^{\infty} r^3 P(r) \, dr} \qquad 3$$

where $P(r)$ is the number-based droplet size distribution of inner droplets, which can be described by a logarithmic normal distribution [5,15]:

$$P(r) = \frac{1}{\sqrt{2\pi} \, 2r\sigma} \, e^{-\frac{\left[\ln \frac{2r}{d_{50}} \right]^2}{2\sigma^2}} \qquad 4$$

where d_{50} is the median and σ the standard deviation of the distribution, which are the fitted parameters, as well as the effective diffusion coefficient of the external water phase, D_e, when solving equations 1-4 simultaneously. Note that if $P(r)$ is interpreted as a volume distribution, there is no multiplication by r^3 in equation 3; and the mean diameter becomes a volume-related median.

Model adaptation to predict a bi-modal size distribution of inner droplets. In order to be able to predict a bimodal size distribution of inner droplets, two lognormal distributions are considered, as suggested by van Duynhoven et al. (2002) [25] and Peña and Hirasaki (2003) [26]:

$$P(r) = \frac{p_{\text{mix}}}{\sqrt{2\pi}2\,r\sigma_1}\,e^{-\frac{\left[\ln\frac{2r}{d_{50,1}}\right]^2}{2\,\sigma_1^2}} + \frac{1-p_{\text{mix}}}{\sqrt{2\pi}\,r\sigma_2}\,e^{-\frac{\left[\ln\frac{2r}{d_{50,2}}\right]^2}{2\,\sigma_2^2}} \qquad 5$$

where p_{mix} is the is the mixing proportion (between 0 and 1) of each lognormal distribution. A specific mean diameter ($d_{50,i}$) and standard deviation (σ_i) is used to describe each population ($i = 1,2$). Equations 1, 3 and 5 are inserted into equation 2 to calculate the total attenuation by the model, E_p. By comparison to the real attenuation, $E_p = I/I_0$, the six tuning parameters were fitted.

3.2 Phenomenological model of droplets swelling and release

A double emulsion is composed of a dispersion of inner droplets within outer droplets. The size distribution of each population can be modeled by a population balance model (PBM). Each PBM should account for the phenomena affecting the size or concentration of droplets. Focusing on the storage of double emulsions, the phenomena that may occur are the coalescence of inner and/or outer droplets, Ostwald ripening and shrinkage or swelling of inner and so of the outer droplets [37–42]. Moreover, the release of the encapsulated substance can take place either by molecular diffusion of the encapsulated substance to the

external phase or by coalescence of the inner droplet with the external phase, called "escape" [3,5,42–46]. When the solubility of the substance used in the oil phase in W/O/W double emulsion is low, the release is governed only by escape (i.e. molecular diffusion of the encapsulated substance in oil is negligible). Furthermore, when a high amount of stabilizer is used, droplet coalescence can be reduced. Thus, in the studied system, it was found that coalescence and Oswald ripening were negligible [27]. The phenomena that occur in the present system are therefore droplet swelling and escape. A coupled PBM model of inner and outer droplet sizes was recently proposed for this system [27], and is summarized below. The objective of this paper is to compare the predictions of the inner DSD by this model with the experimental data from PFG-NMR treated by the GPD approximation involving a bimodal distribution presented above, and to demonstrate the occurrence of swelling of only a fraction of the inner droplets during storage.

The PBM representing the change in the number density function of the inner droplets, n_μ (m^{-3}, i.e. per inner droplet size), and of the outer droplets, n_M (m^{-3}, i.e. per outer droplet size) are given by [27]:

$$\frac{\partial n_\mu(t,v_\mu)}{\partial t} + \frac{\partial\left(\mathbb{S}_\mu(t,v_\mu)n_\mu(t,v_\mu)\right)}{\partial v_\mu} = \Re_{es,\mu}(t,v_\mu) \qquad\qquad 6$$

$$\frac{\partial n_M(t,v_M)}{\partial t} + \frac{\partial\left([\mathbb{S}_M(t,v_M)+Q_{es,M}(t,v_M)]n_M(t,v_M)\right)}{\partial v_M} = 0 \qquad\qquad 7$$

where v (m^3) is the droplet volume. The properties of the inner and outer droplets are indicated by the indices μ and M, respectively. $\Re_{es,\mu}$ ($m^{-3}\,s^{-1}$) is the escape rate of the inner droplets, which causes a change in the outer droplet volume, represented by $Q_{es,M}$ ($m^3\,s^{-1}$). $\mathbb{S}_\mu$ ($m^3\,s^{-1}$) is the volumetric swelling rate of the inner droplets that leads to swelling of the outer droplets, represented by $\mathbb{S}_M$ ($m^3\,s^{-1}$).

Swelling model. Modeling the swelling in W/O/W double emulsions was first done by Matsumoto et al. [41,47–49] who used the membrane permeability model to determine the permeation coefficient of oil layer. This approach has been used frequently to investigate different effects on swelling, including the fraction of the inner phase [48], the fraction of ions (i.e., osmotic pressure) [41,47,48], the fraction of the internal emulsifier [41,47,48] and the oil viscosity [41,47,48]. However, the Laplace pressure was not accounted for in this model, while it can be significant for small inner droplets. The Laplace pressure counterbalances the osmotic pressure, and so the swelling rate. For instance, Guan et al. (2010) [13] reported the occurrence of lower molecular exchange for smaller inner droplets. Based on the membrane permeability model describing the swelling [42,48,50], and including the Laplace pressure and the full size distribution, the volumetric swelling rate of an inner droplet, $\mathbb{S}_\mu$ (m^3 s^{-1}), can be written as follows [27]:

$$\mathbb{S}_\mu(t, v_\mu) = \frac{dv_\mu}{dt} = L_p A_\mu(v_\mu)[\Delta\Pi - \Delta P(v_\mu)]$$ 8

where L_p is the permeability coefficient (m^2 s kg^{-1}) of the membrane, A the droplet surface area (m^2), and $\Delta\Pi$ and ΔP are osmotic and Laplace pressures (Pa), respectively.

By integrating the swelling rates of the encapsulated inner droplets, the swelling rate of the outer droplets, $\mathbb{S}_M$ (m^3 s^{-1}), can be defined as:

$$\mathbb{S}_M(t, v_M) = \frac{v_M}{V_M(t)} \int_0^\infty n_\mu(t, v_\mu)\, \mathbb{S}_\mu(t, v_\mu)\, dv_\mu$$ 9

where V_M is the total volume of the outer droplets.

The sub-models required to complete this model can be found in Appendix A.

4. Results and discussions

The W/O/W double emulsions were stored for one week and then the outer DSD and NMR measurements were performed. Both the mono- and bimodal GPD approaches were

11

applied. Finally, the phenomenological PBM swelling and escape model was used to predict the inner and outer DSDs and the results were compared to the NMR measurements.

Fig. 1 compares the initial and final DSD of the outer droplets measured by laser diffraction. It can be seen that the size distribution of the outer droplets shifts towards bigger sizes. This increase in the size was mainly found to be due to inner (and so outer) droplet swelling, as coalescence and Oswald ripening were found to be negligible in comparable single emulsions [24]. The figure also shows the results of the phenomenological PBM swelling-escape model. The model allows prediction of the swelling of droplets correctly. Note that the swelling model contains parameters that were identified from a set of experiments, under comparable conditions (i.e., same oil, salt, size ranges), giving a permeability coefficient L_p = 2.75 × 10^{-15} and a volume fraction of the critical region from which the droplets can escape α_{cr} = 3.6 × 10^{-5}, [27].
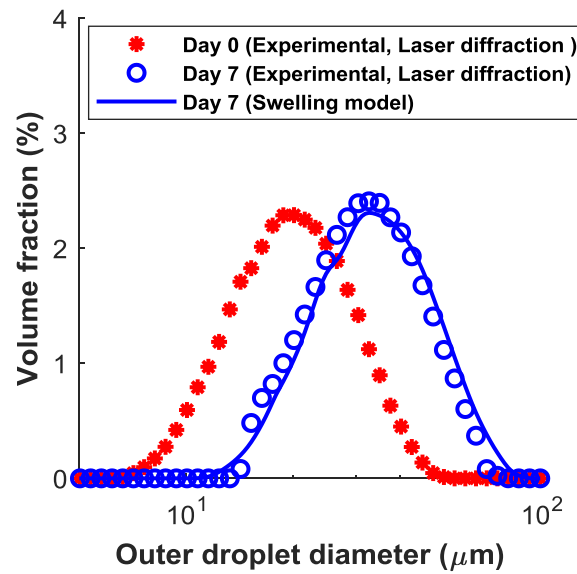

Fig. 1. Evolution of the size distribution of the outer droplets during the first week of storage, for a double emulsion prepared with ϕ_{inner} = 30 % and ϕ_{outer} = 10 %.

4.1 GPD approach based on a monomodal distribution to predict the inner DSD from PFG-NMR

After one week of storage, which corresponds to the time where the maximum swelling of the outer droplets was observed by laser diffraction, the NMR measurement was performed to predict the DSD of inner droplets.

Fig. 2a shows the spectra of the $W_1/O/W_2$ double emulsion as a function of the gradient power. A decay of the 1H signal of water is observed when increasing gradient power. Indeed, at low gradient amplitudes, the outer as well as the inner water phases contribute to the NMR water signal, while at larger gradient amplitudes only the inner water phase contributes to the spectra. An example of a spectrum from the first gradient step is shown by Fig. 2b, indicating the oil and water chemical shift resolution.
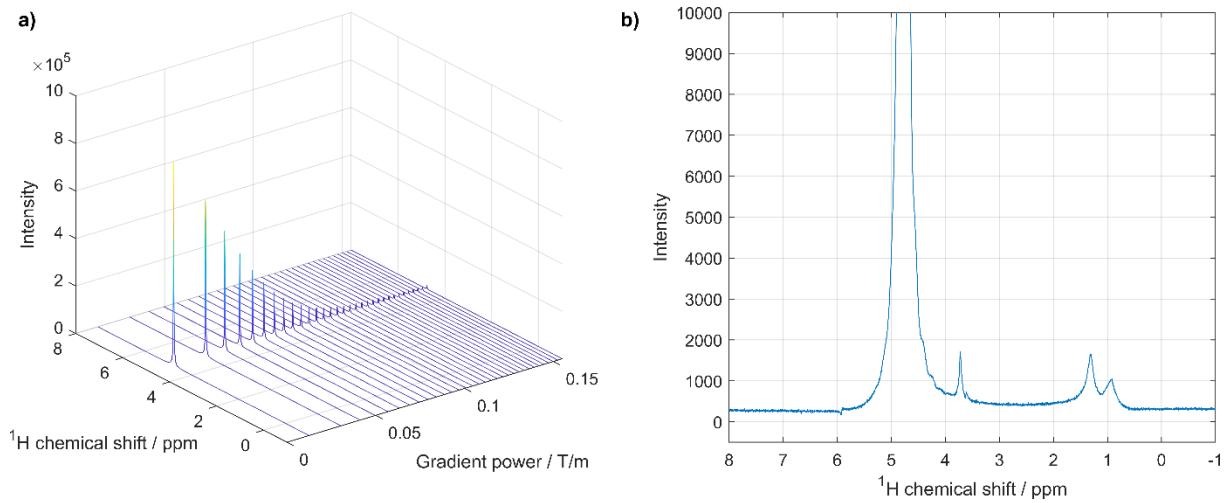

Fig. 2. a) Evolution of the NMR spectra in the $W_1/O/W_2$ double emulsion as a function of the gradient amplitude. b) The spectrum acquired from the first gradient power applied, the y-axis has been cropped so that the water and oil signal chemical shift resolution can be seen.

In order to predict the inner DSD, first of all, the classic GPD approach was used to treat the attenuation signal based on a monomodal lognormal distribution. Equations 1 – 4 were solved while fitting the fitting parameters, leading to $\sigma = 0.22$, $d_{50} = 7.44$ µm and

$D_e = 1.5 \times 10^{-9}$ m² s⁻¹ (Fig. 3). Fig. 3A shows the fitting results of the normalized signal attenuation as a function of q^2 (with $q = \gamma g \delta$). The contribution of free water to signal attenuation is plotted, $\exp\left(-\gamma^2 g^2 D_e \left\{\delta^2 \left(\Delta - \frac{\delta}{3}\right) + \frac{\varepsilon^3}{30} - \frac{\delta\varepsilon^2}{6}\right\}\right)$[22]. It can be seen that its contribution is mainly important at small gradients, but becomes negligible at high gradients. This confirms the necessity to employ an exchange model accounting for both free and restricted diffusions.

Fig. 3B shows the inner DSD. The initial DSD was measured after the preparation of the primary emulsion by light scattering with dilution in oil, as it consists of a single W/O emulsion. The final DSD of inner droplets is predicted by two methods: the monomodal GPD approach and the phenomenological PBM swelling-escape model that allows prediction of the swelling rate of inner droplets. This PBM model predicts a bimodal distribution of the inner droplets. This can be explained by the fact that some of the inner droplets stop swelling as they reach an equilibrium between the Osmotic pressure gradient and Laplace pressure. Therefore, only a fraction of the inner droplets continues to swell, which is approximated by the swelling model to be less than 5 % in number. It can be seen that the GPD approach allows a good prediction of the big population of the inner droplets, which should have a higher impact on the NMR measurement due to their larger number. Even though the GPD approach does not predict the smaller inner droplets, it allows validation of the swelling model and confirms the predicted size of the bigger droplets after one week of storage. The source of difference between the two predictions is due to the employment of a monomodal lognormal distribution in the GPD approach and can be improved by considering a bimodal distribution as done in the next section.
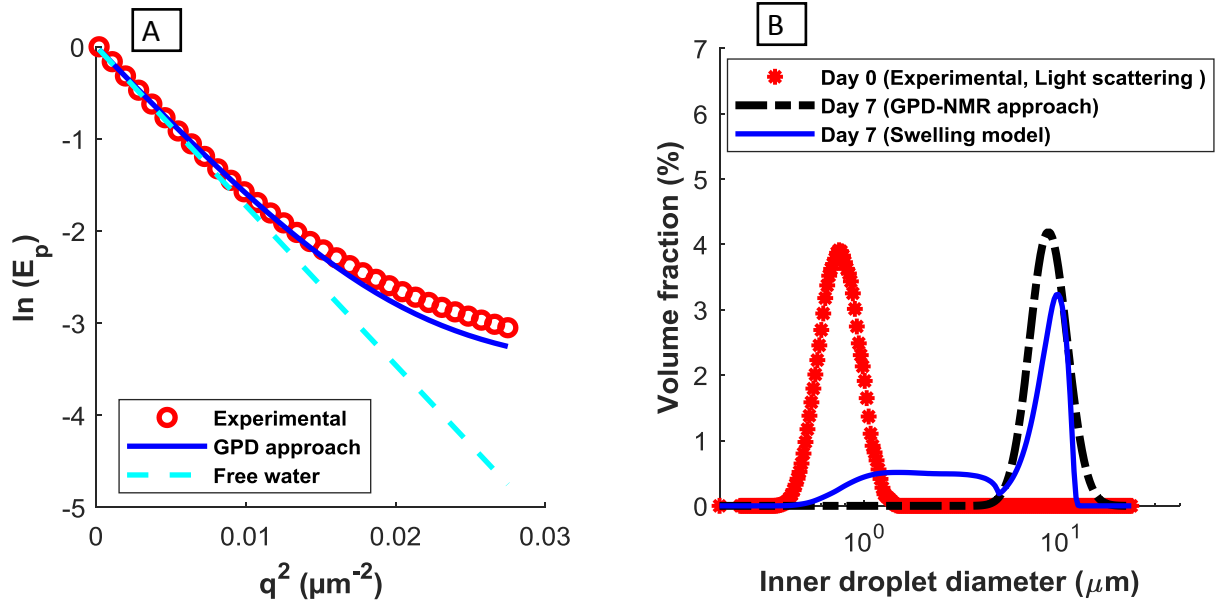
Fig. 3. A) Normalized signal attenuation in log as a function of $q^2 = (\gamma g \delta)^2$. B) Size distribution of the inner droplets. The double emulsion is prepared with ϕ_{inner} = 30 % and ϕ_{outer} = 10 %. The fit of the GPD approach is done using eqs 1–3: σ = 0.22, d_{50}= 7.44 µm and D_e=1.5×10^{-9} m² s^{-1}.

4.2 Bi-model GPD approach to predict the inner DSD from PFG-NMR measurements

In this section, the model suggested by Peña and Hirasaki (2003) [26] (see section 3.1) was used in order to be able to predict a bimodal size distribution of inner droplets, each described by a lognormal distribution. By fitting the bimodal GPD model to the NMR measurements, using eq. 4 instead of eq. 3, the new parameters were identified to be p_{mix} = 0.96, σ_1 = 0.5, $d_{50,1}$ = 1.6 µm, σ_2 = 0.16, and $d_{50,2}$ = 8.4 µm. As can be seen in Fig. 4B the NMR approach allows prediction of a bimodal inner size distribution. The GPD predictions are now in line with the predictions of the swelling model, with a good estimate of both amplitudes. The PGF-NMR combined with the bimodal GPD treatment can thus be used as an experimental method to predict the inner DSD and therefore to validate the PBM swelling-escape model.
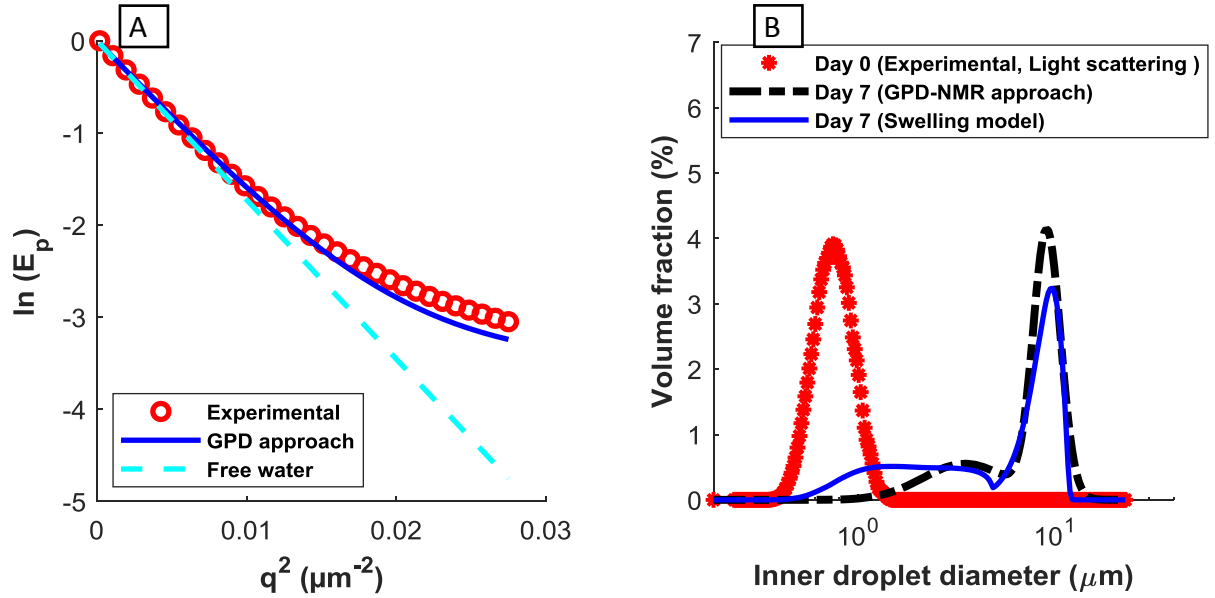
15

Fig. 4. A) Normalized signal attenuation in log as a function of $q^2 = (\gamma g \delta)^2$. B) Size distribution of the inner droplets. The double emulsion is prepared with ϕ_{inner} = 30 % and ϕ_{outer} = 10 %. The fit of the GPD approach is done using eqs. 1, 2, and 4: p_{mix} = 0.96, σ_1 = 0.5, $d_{50,1}$ = 1.6 µm, σ_2 = 0.16, $d_{50,2}$ = 8.4 µm and D_e=1.5×10^{-9}.

4.3 Investigation of the NMR operating conditions

The gradient pulse duration (δ) was varied from 4 ms to 10 ms, and a better prediction was obtained with 4 ms that was conserved. Similarly, the number of steps of variation of g was changed between 8 and 32 steps, and a finer prediction was obtained with 32 steps that was conserved.

The effect of the gradient pulse delay or diffusion time (Δ) can be observed on Fig. 5 for two samples with different inner oil fractions. As well known, increasing Δ leads to a faster decay in E_p. However, a lower precision is obtained at very high Δ, therefore values between 100 and 200 ms are recommended in this application. Interestingly, the prediction of the bimodal distribution was identical with the different values of Δ, which demonstrates the robustness of the predictions to this parameter.
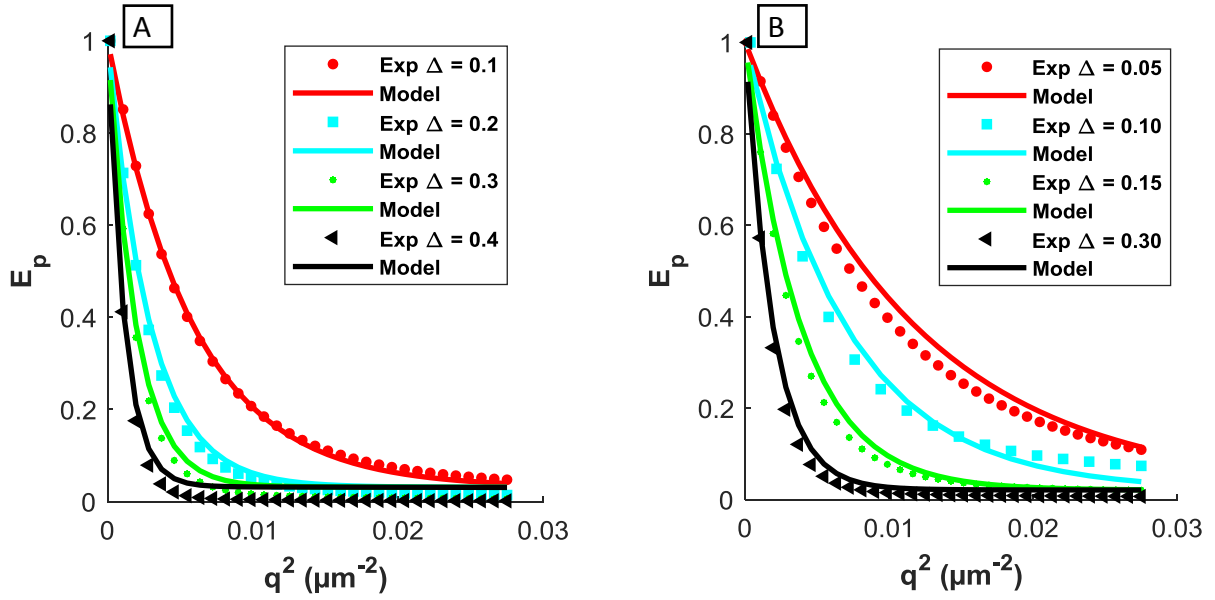
Fig. 5. Normalized signal attenuation as a function of $q^2 = (\gamma g \delta)^2$ for different gradient pulse delays Δ: A) 2.17% inner phase B) 3.23% inner phase.

The double emulsion was first stored at room temperature for one week where swelling occurred. Then it was measured by NMR (day 7 in Fig. 6) and stored in fridge (5°C) and measured again at days 10 and 15. Figure 6 shows that the sample did not undergo further swelling at 5°C.
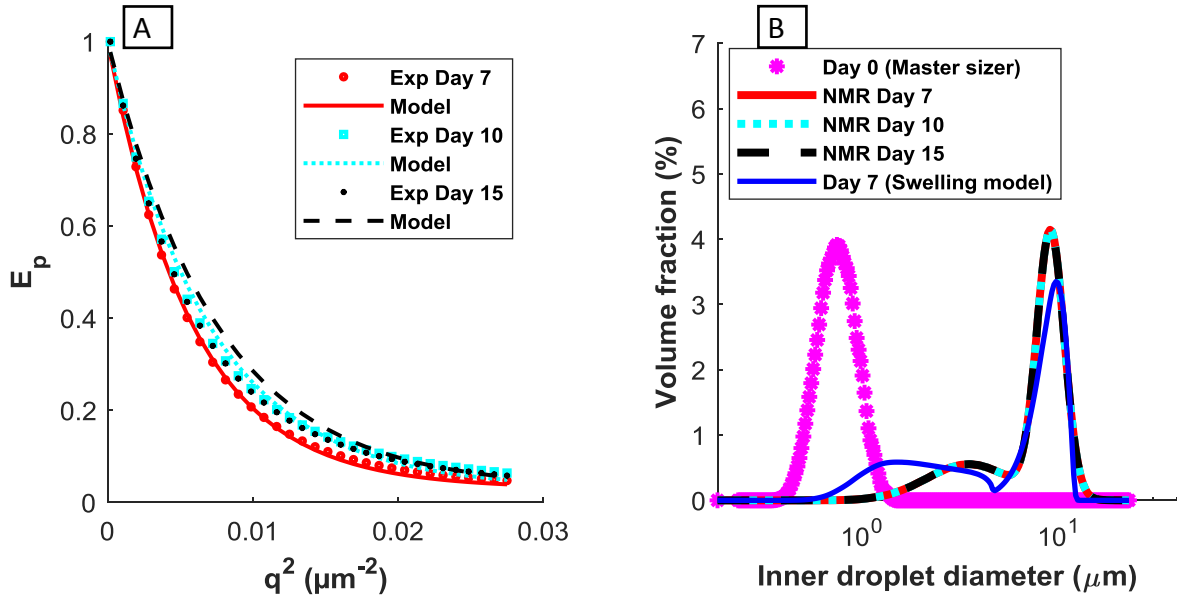

Fig. 6. Effect of storage time A) Normalized signal attenuation as a function of q^2. B) Size distribution of the inner droplets.

4.4 Prediction of the interfacial tension

One important parameter necessary in the swelling model is the interfacial tension between the outer droplets and the internal phase. This parameter governs the Laplace pressure, which counterbalances the Osmotic pressure gradient. It thus determines the fraction of droplets that continue to swell. However, measuring the interfacial tension of the outer droplets (for instance by the optical pendant drop method) might be subject to error due to the fact that outer droplets are themselves emulsions and the use of a mixture of hydrophilic and hydrophobic emulsifiers. The NMR predictions can be useful in validating such parameters in the phenomenological model.

Fig. 7 shows that when varying the interfacial tension, the population of big inner droplets is not well predicted by the PBM swelling-escape model. The NMR measurement and the proposed GPD approach thus allow the validation of the swelling model and the employed parameters. The predicted size is consistent with qualitative optical observations of this double emulsion [24].
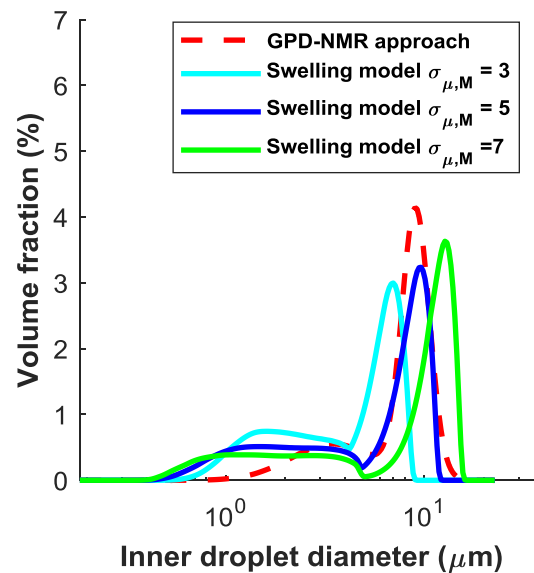

Fig. 7. Effect of interfacial tension ($\sigma_{\mu,M}$, N m^{-1}) on inner size distribution obtained by swelling model.

5. Conclusions

The well-known Gaussian Phase Distribution approach was modified to predict bimodal droplet size distributions of inner droplets in W/O/W double emulsions. The results were compared to a phenomenological model based on a coupled PBM approach of inner and outer droplet size distributions, involving swelling and escape. These two phenomena are known to occur in double emulsions during storage and are important to predict as they affect the product quality and stability. Both methods indicate the occurrence of a bimodal distribution of the inner droplets after a week of storage, which can be explained by the differences in Laplace pressure between small droplets and bigger droplets. This leads to the fact that when swelling occurs, the concentration of salt inside the inner droplets decreases, which decreases the osmotic pressure that becomes lower than the Laplace pressure for smaller droplets.

Appendix A

Swelling model. The osmotic pressure gradient between the internal and external aqueous phases, $\Delta\Pi$ (Pa), is defined as [51,52]:

$$\Delta\Pi = \Pi_{in} - \Pi_{out} = i\,R\,T\,(C_{in} - C_{out}) \qquad\qquad\qquad\qquad A1$$

where i is the van't Hoff factor (~2 for NaCl [51]) , R (J K^{-1} mol^{-1}) the universal gas constant, T (K) temperature and C (mol m^{-3}) the concentration of salt in which "in" and "out" indicates the inner and outer water phases, respectively.

The Laplace pressure for the inner droplets, ΔP (Pa), is:

$$\Delta P(v_\mu) = \frac{4\,\sigma_{\mu,M}}{d_\mu} \qquad\qquad\qquad\qquad A2$$

where d (m) is the droplets diameter and $\sigma_{\mu,M}$ (N m^{-1}) the interfacial tension between inner and outer droplets.

Escape model. Different approaches have proposed in the literature to describe inner droplet escape [43,53,54]. The general form assumes the escape rate to be proportional to the escape frequency (or frequency of collision of inner droplets with the outer droplet surface), the escape probability and a critical region from which inner droplets may escape. A model was recently proposed and validated experimentally by Khadem and Sheibat-Othman [27], where the escape rate of inner droplets, $\mathfrak{R}_{es,\mu}$(m^{-3} s^{-1}) is given by:

$$\mathfrak{R}_{es,\mu}(t, v_\mu) = -\alpha_{cr}\, n_\mu(t, v_\mu)\, \frac{1}{N_M} \int_0^\infty \Omega_{es}(v_\mu, v_M) n_M(t, v_M)\, dv_M \qquad \text{A3}$$

where N_M is the total number of outer droplets, Ω_{es} (s^{-1}) is the escape frequency, α_{cr} is the volume fraction of the critical region from which the droplets can escape.

As a consequence of the overall escape rate of inner droplets from each outer droplet, a volumetric decrease in the outer droplet size, $Q_{es,M}$ (m^3 s^{-1}), is obtained:

$$Q_{es,M}(t, v_M) = \frac{v_M}{V_M(t)} \int_0^\infty \mathfrak{R}_{es,\mu}(t, v_\mu)\, v_\mu\, dv_\mu \qquad \text{A4}$$

The escape frequency is defined as $\Omega_{es} = 1/t_{es}(v_\mu, v_M)$ (s^{-1}), with t_{es} (s) the escape time. In this work, t_{es} is determined using the approach of Kang et al. (2016) based on the momentum and energy conservations in stoke flow [55,56]:

$$t_{es}(v_\mu, v_M) = \int_{0.01}^{L_{eq}} \frac{1}{u_\mu(v_\mu) + u_M(v_M)}\, dL \qquad \text{A5}$$

where u (m s^{-1}) is the velocity, $L = 2\, l/d_\mu$ a dimensionless position and L_{eq} the final position of the inner droplet at equilibrium with $L_{eq} = 2$ for escape (i.e., when $l = d_\mu$ the complete separation occurs). 0.5 % of d_μ is considered as a threshold of escape, which gives a lower bound of the integral of L of 1 %.

In case of negligible continuous phase viscosity in comparison to that of the outer droplet, the momentum conservation gives:

$$m_\mu \, u_\mu(v_\mu) = m_M \, u_M(v_M) \qquad \text{A6}$$

Where m (kg) is the droplet's mass.

Kang et al., defined the driving force of separation (F_S) during the escape process as:

$$F_S(v_\mu, v_M) = \pi \, d_\mu \, L(2 - L)\sigma_{\mu,M} \left(1 - \frac{\sigma_{\mu,out}}{\sigma_{\mu,M}} + \frac{\sigma_{M,out}}{\sigma_{\mu,M}} \frac{1}{K}\right) \qquad \text{A7}$$

where $K = \frac{d_M}{d_\mu}$ and the interfacial tensions is considered across the three phases – i.e., the inner droplet with outer droplet ($\sigma_{\mu,M}$), the outer droplet with the outer continuous phase ($\sigma_{M,out}$) and the inner droplet with the outer continuous phase ($\sigma_{\mu,out}$, null in the present work).

The resistance force to escape (F_V) is considered to be governed by the outer droplet viscosity:

$$F_V(v_\mu, v_M) = \frac{3}{2}\pi \, d_\mu \eta_M \left[u_\mu(v_\mu) + u_M(v_M)\right](2 - L) \qquad \text{A8}$$

Finally, energy conservation implies:

$$\int_{0.01}^{L}\left[F_S(v_\mu, v_M) - F_V(v_\mu, v_M)\right]dL = \frac{1}{2}m_\mu u_\mu^2(v_\mu) + \frac{1}{2}m_M u_M^2(v_M) \qquad \text{A9}$$

Acknowledgement

Data access: "All experimental NMR data reported in this work is available via University of Strathclyde's KnowledgeBase at https://doi.org/10.15129/e5c7d5ba-8e84-41ce-984d-d9a8fbac4636."

References

[1] G. Muschiolik, *Curr. Opin. Colloid Interface Sci.* **2007**, *12* (4–5), 213–220. DOI: 10.1016/j.cocis.2007.07.006.

[2] A. Aserin, Ed. , *Multiple Emulsions: Technology and Applications*, Wiley-Interscience, Hoboken, N.J **2008**.

[3] W. S. W. Ho, K. K. Sirkar, Eds. , *Membrane Handbook*, Springer US, Boston, MA **1992**.

[4] S. Matsumoto, Y. Kita, D. Yonezawa, *J. Colloid Interface Sci.* **1976**, *57* (2), 353–361. DOI: 10.1016/0021-9797(76)90210-1.

[5] F. Wolf, L. Hecht, H. P. Schuchmann, E. H. Hardy, G. Guthausen, *Eur. J. Lipid Sci. Technol.* **2009**, *111* (7), 730–742. DOI: 10.1002/ejlt.200800272.

[6] R. Bernewitz, U. S. Schmidt, H. P. Schuchmann, G. Guthausen, *Colloids Surf. Physicochem. Eng. Asp.* **2014**, *458*, 10–18. DOI: 10.1016/j.colsurfa.2014.01.002.

[7] R. Bernewitz, F. Dalitz, K. Köhler, H. P. Schuchmann, G. Guthausen, *Microporous Mesoporous Mater.* **2013**, *178*, 69–73. DOI: 10.1016/j.micromeso.2013.02.049.

[8] S. Schuster, R. Bernewitz, G. Guthausen, J. Zapp, A. M. Greiner, K. Köhler, H. P. Schuchmann, *Chem. Eng. Sci.* **2012**, *81*, 84–90. DOI: 10.1016/j.ces.2012.06.059.

[9] M. L. Johns, K. G. Hollingsworth, *Prog. Nucl. Magn. Reson. Spectrosc.* **2007**, *50* (2–3), 51–70. DOI: 10.1016/j.pnmrs.2006.11.001.

[10] J. S. Murday, R. M. Cotts, *J. Chem. Phys.* **1968**, *48* (11), 4938–4945. DOI: 10.1063/1.1668160.

[11] K. J. Packer, C. Rees, *J. Colloid Interface Sci.* **1972**, *40* (2), 206–218. DOI: 10.1016/0021-9797(72)90010-0.

[12] J. P. Hindmarsh, J. Su, J. Flanagan, H. Singh, *Langmuir.* **2005**, *21* (20), 9076–9084. DOI: 10.1021/la051626b.

[13] X. Guan, K. Hailu, G. Guthausen, F. Wolf, R. Bernewitz, H. P. Schuchmann, *Eur. J. Lipid Sci. Technol.* **2010**, *112* (8), 828–837. DOI: 10.1002/ejlt.201000022.

[14] L. Vermeir, P. Sabatino, M. Balcaen, A. Declerck, K. Dewettinck, J. C. Martins, G. Guthausen, P. Van der Meeren, *J. Colloid Interface Sci.* **2016**, *475*, 57–65. DOI: 10.1016/j.jcis.2016.04.029.

[15] I. Lönnqvist, B. Håkansson, B. Balinov, O. Söderman, *J. Colloid Interface Sci.* **1997**, *192* (1), 66–73. DOI: 10.1006/jcis.1997.4966.

[16] B. Balinov, B. Jonsson, P. Linse, O. Soderman, *J. Magn. Reson. A.* **1993**, *104* (1), 17–25. DOI: 10.1006/jmra.1993.1184.

[17] D. C. Douglass, D. W. McCall, *J. Phys. Chem.* **1958**, *62* (9), 1102–1107.

[18] A. V. Barzykin, *J. Magn. Reson.* **1999**, *139* (2), 342–353. DOI: 10.1006/jmre.1999.1778.

[19] M. A. Voda, J. van Duynhoven, *Trends Food Sci. Technol.* **2009**, *20* (11–12), 533–543. DOI: 10.1016/j.tifs.2009.07.001.

[20] J. Pfeuffer, U. Flögel, W. Dreher, D. Leibfritz, *NMR Biomed.* **1998**, *11* (1), 19–31. DOI: 10.1002/(SICI)1099-1492(199802)11:1<19::AID-NBM499>3.0.CO;2-O.

[21] W. S. Price, *Concepts Magn. Reson. Educ. J.* **1997**, *9* (5), 299–336.

[22] W. S. Price, A. V. Barzykin, K. Hayamizu, M. Tachiya, *Biophys. J.* **1998**, *74* (5), 2259–2271. DOI: 10.1016/S0006-3495(98)77935-4.

[23] L. Vermeir, M. Balcaen, P. Sabatino, K. Dewettinck, P. Van der Meeren, *Colloids Surf. Physicochem. Eng. Asp.* **2014**, *456*, 129–138. DOI: 10.1016/j.colsurfa.2014.05.022.

[24] B. Khadem, M. Khellaf, N. Sheibat-Othman, *Colloids Surf. Physicochem. Eng. Asp.* **2020**, *585*, 124181. DOI: 10.1016/j.colsurfa.2019.124181.

[25] J. P. M. van Duynhoven, G. J. W. Goudappel, G. van Dalen, P. C. van Bruggen, J. C. G. Blonk, A. P. A. M. Eijkelenboom, *Magn. Reson. Chem.* **2002**, *40* (13), S51–S59. DOI: 10.1002/mrc.1115.

[26] A. A. Peña, G. J. Hirasaki, *Adv. Colloid Interface Sci.* **2003**, *105* (1–3), 103–150. DOI: 10.1016/S0001-8686(03)00092-7.

[27] B. Khadem, N. Sheibat-Othman, *Chem. Eng. J.* **2020**, *382*, 122824. DOI: 10.1016/j.cej.2019.122824.

[28] W. S. Price, *Concepts Magn. Reson.* **1998**, 197–237.

[29] B. Blümich, *TrAC Trends Anal. Chem.* **2016**, *83*, 2–11. DOI: 10.1016/j.trac.2015.12.012.

[30] K. Meyer, S. Kern, N. Zientek, G. Guthausen, M. Maiwald, *TrAC Trends Anal. Chem.* **2016**, *83*, 39–52. DOI: 10.1016/j.trac.2016.03.016.

[31] N. N. A. Ling, A. Haber, E. F. May, E. O. Fridjonsson, M. L. Johns, *Chem. Eng. Sci.* **2017**, *160*, 362–369. DOI: 10.1016/j.ces.2016.11.045.

[32] N. N. A. Ling, A. Haber, T. J. Hughes, B. F. Graham, E. F. May, E. O. Fridjonsson, M. L. Johns, *Energy Fuels*. **2016**, *30* (7), 5555–5562. DOI: 10.1021/acs.energyfuels.6b00782.

[33] E. O. Fridjonsson, B. F. Graham, M. Akhfash, E. F. May, M. L. Johns, *Energy Fuels*. **2014**, *28* (3), 1756–1764. DOI: 10.1021/ef402117k.

[34] I. A. Lingwood, T. C. Chandrasekera, J. Kolz, E. O. Fridjonsson, M. L. Johns, *J. Magn. Reson.* **2012**, *214*, 281–288. DOI: 10.1016/j.jmr.2011.11.020.

[35] E. O. Stejskal, J. E. Tanner, *J. Chem. Phys.* **1965**, *42* (1), 288–292. DOI: 10.1063/1.1695690.

[36] M. Holz, S. R. Heil, A. Sacco, *Phys. Chem. Chem. Phys.* **2000**, *2* (20), 4740–4742. DOI: 10.1039/b005319h.

[37] L. Zeng, Y. Zhang, C. Bukirwa, W. Li, Y. Yang, *RSC Adv.* **2015**, *5* (109), 89959–89970. DOI: 10.1039/C5RA16267J.

[38] J. Yan, R. Pal, *J. Membr. Sci.* **2003**, *213* (1–2), 1–12. DOI: 10.1016/S0376-7388(02)00501-X.

[39] R. M. Pfeiffer, A. L. Bunge, W. Navidi, *Sep. Sci. Technol.* **2003**, *38* (3), 519–539. DOI: 10.1081/SS-120016649.

[40] S. Mukhopadhyay, S. K. Ghosh, V. A. Juvekar, *Desalination*. **2008**, *232* (1–3), 110–127. DOI: 10.1016/j.desal.2008.01.009.

[41] S. Mataumoto, W. W. Kang, *J. Dispers. Sci. Technol.* **1989**, *10* (4–5), 455–482. DOI: 10.1080/01932698908943184.

[42] N. Jager-Lezer, I. Terrisse, F. Bruneau, S. Tokgoz, L. Ferreira, D. Clausse, M. Seiller, J.-L. Grossiord, *J. Controlled Release*. **1997**, *45* (1), 1–13. DOI: 10.1016/S0168-3659(96)01507-6.

[43] M. Chávez-Páez, C. M. Quezada, L. Ibarra-Bracamontes, H. O. González-Ochoa, J. L. Arauz-Lara, *Langmuir*. **2012**, *28* (14), 5934–5939. DOI: 10.1021/la205144g.

[44] R. Mezzenga, B. M. Folmer, E. Hughes, *Langmuir*. **2004**, *20* (9), 3574–3582. DOI: 10.1021/la036396k.

[45] T. Schmidts, D. Dobler, C. Nissing, F. Runkel, *J. Colloid Interface Sci.* **2009**, *338* (1), 184–192. DOI: 10.1016/j.jcis.2009.06.033.

[46] A. J. Shere, H. M. Cheung, *Chem. Eng. Commun.* **1988**, *68* (1), 143–164. DOI: 10.1080/00986448808940403.

[47] S. Matsumoto, M. Kohda, *J. Colloid Interface Sci.* **1980**, *73* (1), 13–20.

[48] S. Matsumoto, T. Inoue, M. Kohda, K. Ikura, *J. Colloid Interface Sci.* **1980**, *77* (2), 555–563.

[49] S. Matsumoto, P. Sherman, *J. Texture Stud.* **1981**, *12* (2), 243–257. DOI: 10.1111/j.1745-4603.1981.tb01234.x.

[50] O. Kedem, A. Katchalsky, *Biochim. Biophys. Acta*. **1958**, *27*, 229–246.

[51] O. Karnland, *Bentonite Swelling Pressure in Strong NaCl Solutions. Correlation between Model Calculations and Experimentally Determined Data*, Swedish Nuclear Fuel And Waste Management Co. **1997**.

[52] T. S. H. Leong, M. Zhou, N. Kukan, M. Ashokkumar, G. J. O. Martin, *Food Hydrocoll.* **2017**, *63*, 685–695. DOI: 10.1016/j.foodhyd.2016.10.017.

[53] K. Pays, *J. Controlled Release*. **2002**, *79* (1–3), 193–205. DOI: 10.1016/S0168-3659(01)00535-1.

[54] J. K. Klahn, J. J. M. Janssen, G. E. J. Vaessen, R. de Swart, W. G. M. Agterof, *Colloids Surf. Physicochem. Eng. Asp.* **2002**, *210* (2–3), 167–181. DOI: 10.1016/S0927-7757(02)00376-X.

[55] Z. Kang, P. Zhu, T. Kong, L. Wang, *Micromachines*. **2016**, *7* (11), 196. DOI: 10.3390/mi7110196.

[56] B. Khadem, N. Sheibat-Othman, in *Comput. Aided Chem. Eng.*, Vol. 40, Elsevier **2017**.